The spatial and electronic effects of polypyrrole between MnO_2 layers enhance the diffusion ability of Zn^{2+} ions

Le Li[a], Shaofeng Jia[a], Shi Yue[a], Yuanyuan Yang[a], Chao Tan[b], Conghui Wang[b], Hengwei Qiu[c], Yongqiang Ji[e], Minghui Cao[d], Dan Zhang[b]*

[a] Shaanxi Key Laboratory of Industrial Automation, School of Mechanical Engineering, Shaanxi University of Technology, Hanzhong 723001, China.

[b] Shaanxi Key Laboratory of Catalysis, School of Chemistry and Environment Science, Shaanxi University of Technology, Hanzhong 723001, China.

[c] State Key Laboratory of Alternate Electrical Power System with Renewable Energy Sources, School of New Energy, North China Electric Power University, Beijing 102206, China.

[d] School of Electronic and Information Engineering, Qingdao University, Qingdao 266071, China.

[e] Institute of Physics, Henan Academy of Sciences Zhengzhou, 450046, China.

*Corresponding Authors.

E-mail: zhangdan@snut.edu.cn (Dan Zhang).

1. Material and methods

1.1 Material preparation

Synthesis of PPy: First, 0.72 g of cetyltrimethylammonium bromide (CTAB) was dispersed in 200 ml of deionized water and stirred for 20 minutes. Then, the solution was transferred to an ice bath device at 0−5°C and stirred, and 750 μl of pyrrole solution was added dropwise. After 1 h, 100 ml of $(NH_4)_2S_2O_8$ solution (0.2 M) was added again and stirring was continued for 4 h. Finally, the obtained mixed solution is alternately washed three times with deionized water and absolute ethanol, and then dried in an oven at 60°C for 12 h to obtain the final PPy sample.

Synthesis of δ-MnO_2: First, 1.1376 g of $KMnO_4$ and 0.18 g of $MnSO_4$ were dissolved in 60 ml of deionized water, and the mixture was stirred for 30 min until fully mixed. After that, the sample was placed in a 100 ml high-pressure reaction kettle for hydrothermal treatment at 160°C for 12 h. After cooling to 20−25°C, the sample was washed alternately with deionized water and ethanol three times and finally dried in an oven at 60°C for 12 h to obtain a δ-MnO_2 sample.

Synthesis of MnO_2/PPy-x: First, 1.1376 g of $KMnO_4$ and 0.18 g of $MnSO_4$ were dissolved in 60 ml of deionized water. After complete dissolution, the PPy with mass fractions of 0.5%, 1%, 5%, and 10% were added and stirred for 30 min until fully mixed. After that, the mixed solutions were transferred to a 100 ml high-pressure

reactor and heated at 160℃ for 12 h. After cooling to20−25°C, the samples were washed alternately with deionized water and ethanol 3 times and finally dried at 60℃ in the oven for 12 h to obtain MnO_2/PPy-x samples (MnO_2/PPy-0.5, MnO_2/PPy-1, MnO_2/PPy-5, and MnO_2/PPy-10 containing 0.5%, 1%, 5%, and 10% PPy, respectively).

1.2 Electrochemical test

To evaluate the electrochemical properties of MnO_2/PPy-x samples, CR2032 button cells were prepared. The active MnO_2/PPy-x, conductive carbon black, and polyvinylidene fluoride (PVDF) were mixed at a ratio of 8:1:1, and the mixtures were dissolved in an *N*-methylpyrrolidone (NMP) solvent to make a uniform slurry. The slurry was evenly coated on the graphite foil, and after the resulting samples were vacuum dried at 60℃ for 12 h, the final cathodes were prepared, and its load was about 0.8−1.2 mg. The negative electrode is zinc foil, GF/D glass fiber is used as the diaphragm, and the electrolyte is a 2 M $ZnSO_4$ + 0.2 M $MnSO_4$ solution. The LAND battery test system (CT2001A) was used to perform a galvanostatic charge and discharge (GCD) and GITT. Cyclic voltammetry (CV) and electrochemical impedance (EIS) were performed on the CHI660 electrochemical workstation. The voltage test range is 0.8−1.8 V.

1.3 Material characterization

The crystal structure and composition of the sample were characterized by Bruker D8 Advance X-ray diffractometer (XRD) at Cu-Kα radiation (λ=1.54178 Å) ranging from 10°−80°. The microstructure and element content of the samples were confirmed by SEM (Zeiss Sigma 300). XPS analysis selected Al-Kα radiation (Thermo Fisher, ESCALAB 250Xi) to determine the valence state and functional group of the sample, and calibrated the spectrum with the binding energy of 284.8eV C1s spectral line. The Raman spectra of the samples were measured via the Renishaw InVia system (argon ion laser excitation wavelength is 532 nm) in the range of 200−1000 cm^{-1}. FTIR spectroscopy was performed on the FTIR-920 instrument.

1.4 Calculation method

The study used VASP to calculate density functional theory (DFT) with projector-

augmented wave[1,2]. Electron spin polarization was considered in all calculations. The Perdew-Burke-Ernzerhof functional was employed for exchange-correlation effects[3], while DFT+D3 was used for handling weak interactions[4]. The cut-off energy for the plane-wave basis was 450 eV. K-points were 3*3*1 in the Brillouin zone. 15 Å of layer vacuum was applied at the Z-axis of slab models to avoid the Periodic effect. Energy and maximum stress were converged to 10^{-5} eV and 0.04 eV/Å, respectively.

Adsorption energy was calculated to evaluate the adsorption ability of the catalysts, and the calculation method was shown in Eq. 1[3],

$$E_{ads} = E_{catalysts+adsorbates} - E_{catalysts} - E_{adsorbates} \quad (1)$$

where E_{ads} was the adsorption energy, $E_{catalysts+adsorbates}$ was the total energy after the adsorbates were adsorbed, $E_{catalysts}$ was the catalysts' energy and $E_{adsorbates}$ was the energy of adsorbates.

2. Supplementary Figures

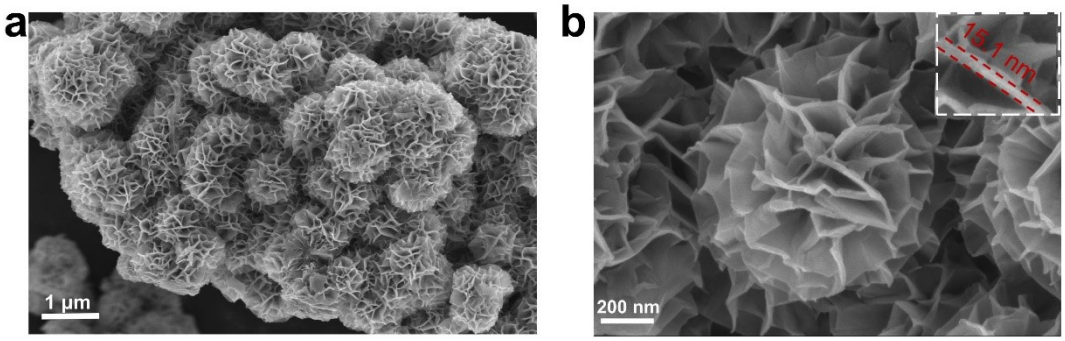

Fig. S1. (a), (b) SEM images of MnO_2 at 1 μm and 200 nm scales.

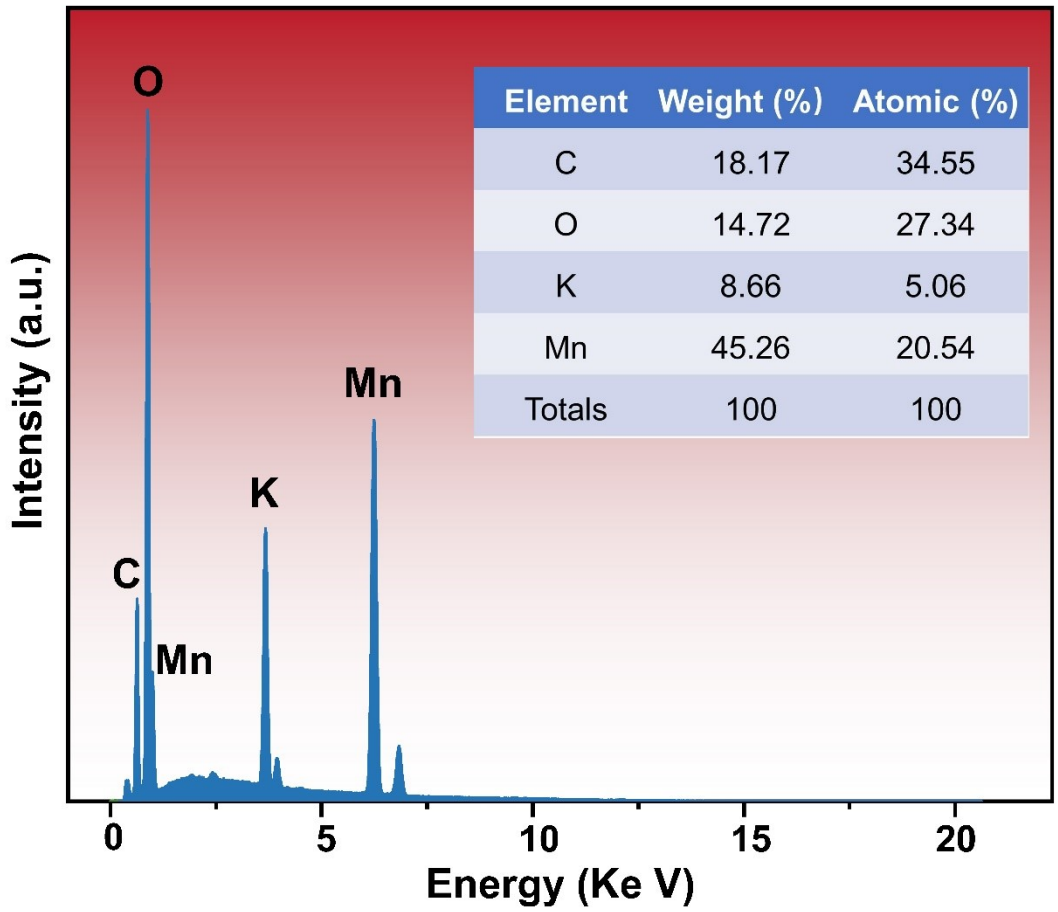

Element	Weight (%)	Atomic (%)
C	18.17	34.55
O	14.72	27.34
K	8.66	5.06
Mn	45.26	20.54
Totals	100	100

Fig. S2. EDX spectrum of MnO_2.

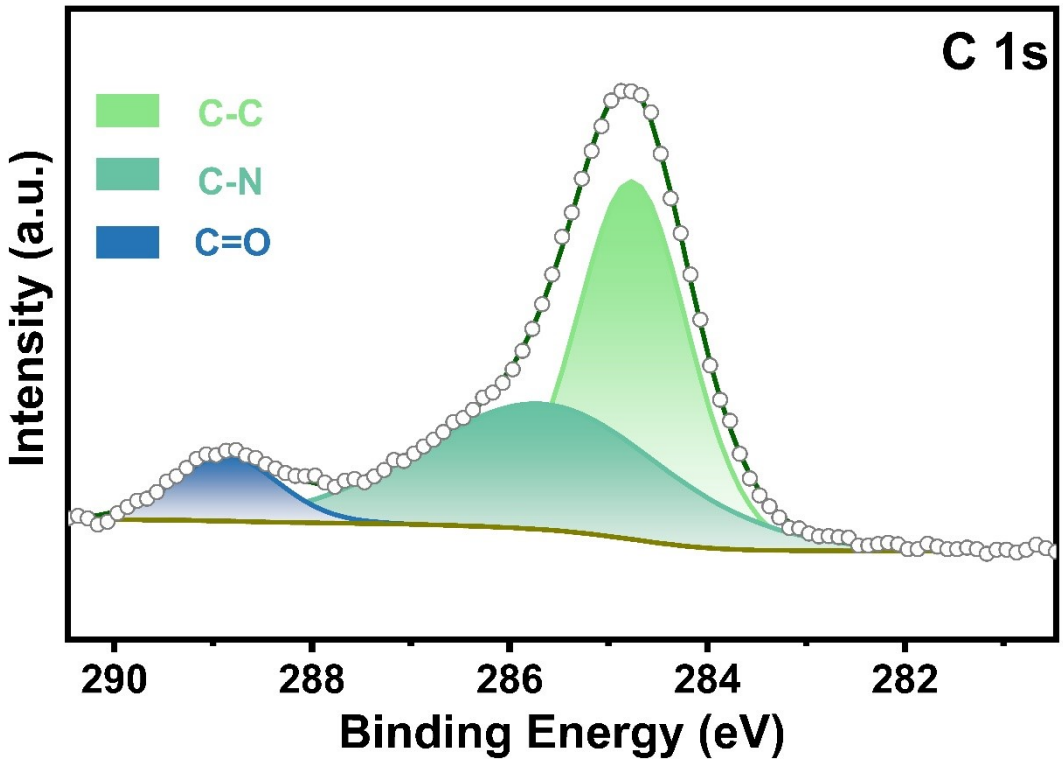

Fig. S3. C 1s spectrum of MnO_2/PPy-1.

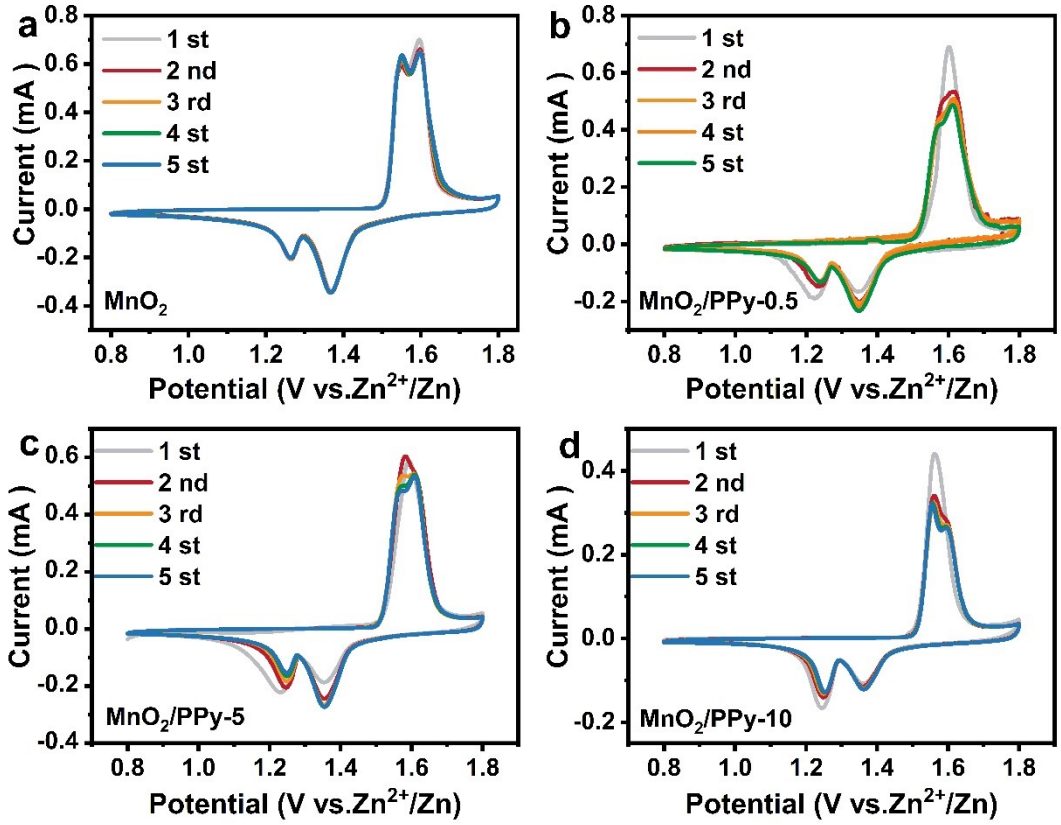

Fig. S4. CV curves of (a) MnO_2, (b) MnO_2/PPy-0.5, (c) MnO_2/PPy-5, and (d) MnO_2/PPy-10 cathode at a scan rate of 0.1 mV s^{-1}.

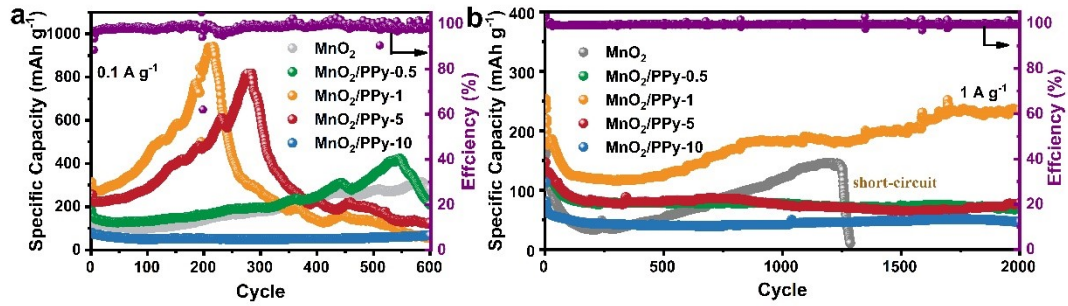

Fig. S5. Cyclic performance of MnO_2 and MnO_2/PPy-x samples at different current densities，(a) 0.1 A g^{-1}. (b) 1 A g^{-1}.

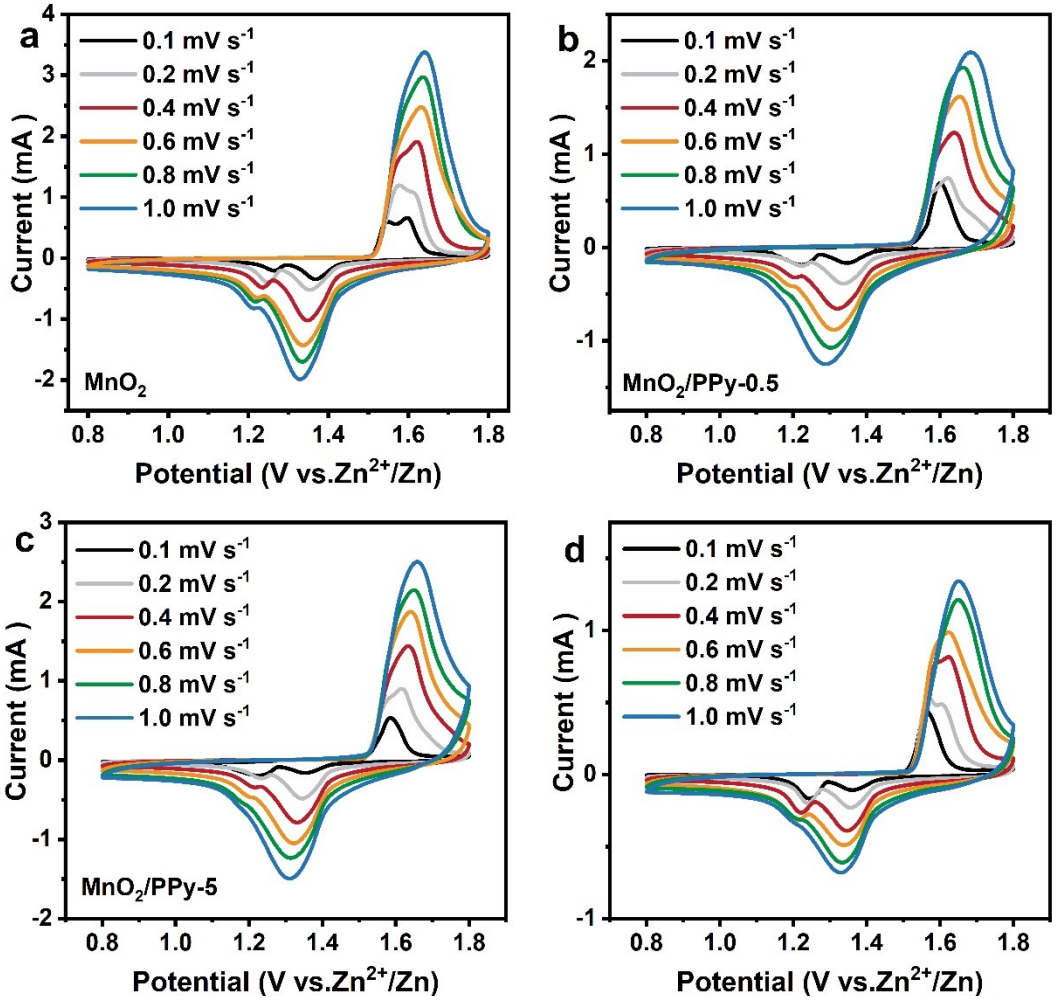

Fig. S6. CV curves of (a) MnO_2, (b) MnO_2/PPy-0.5, (c) MnO_2/PPy-5, and (d) MnO_2/PPy-10 cathode at various scan rates.

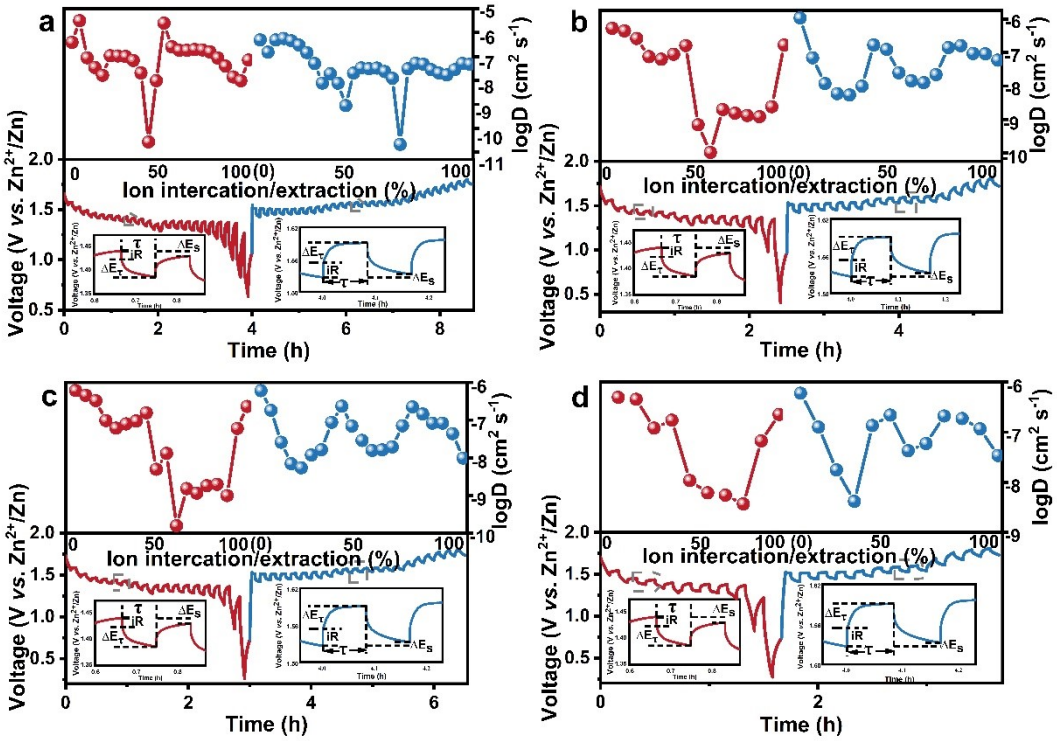

Fig. S7. Diffusion coefficient of (a) MnO_2, (b) MnO_2/PPy-0.5, (c) MnO_2/PPy-5, and (d) MnO_2/PPy-10 cathode.

3. Supplementary Table

Table S1. Electrochemical performance comparison of manganese-based cathode in AZIBs.

Materials	Voltage window (V)	Cycle performance	Cycle	References
VMO-5	0.8−1.8	283 mAh g^{-1} at 1 A g^{-1}	2000	This work
MnO_2-P	1.4−4.4	120 mAh g^{-1} at 1 A g^{-1}	5000	5
δ-MnO_2	0.9−1.8	70 mAh g^{-1} at 3 A g^{-1}	1000	6
F-MO	0.8−1.8	240 mAh g^{-1} at 0.2 A g^{-1}	200	7
PEDOT-MnO_2	0.8−1.8	142 mAh g^{-1} at 2 A g^{-1}	1500	8
MnO_2@PANI	1.0−1.85	343 mAh g^{-1} at 0.2 A g^{-1}	100	9
H-MnO_2	1.0−2.0	97 mAh g^{-1} at 3.8 A g^{-1}	5000	10
Al-MnO_2	1.0−1.8	84 mAh g^{-1} at 2 A g^{-1}	2000	11
Al-KMO	0.8−1.9	270 mAh g^{-1} at 0.5 A g^{-1}	500	12
GNFM	0−2.5	31 mAh g^{-1} at 2.86 C	6000	13

Acronym definitions: PANI intercalated MnO_2 (PMO-10), F doping MnO_2 (F-MO), Hydroxylated MnO_2 (H-MnO_2), Graphite nanoflake/Mxene (GNFM).

References

1. G. Kresse and J. Furthmüller, Efficient iterative schemes for ab initio total-energy calculations using a plane-wave basis set, *Phys. Rev. B Condens Matter.*, 1996, **54**, 11169–11186.
2. P.E. Blöchl, Projector augmented-wave method, *Phys. Rev. B*, 1994, **50**, 17953–17979.
3. J.P. Perdew and K. Burke, M. Ernzerhof, Generalized gradient approximation made simple, *Phys. Rev. Lett*., 1996, **77**, 3865–3868.
4. S. Grimme, J. Antony, S. Ehrlich and H. Krieg, A consistent and accurate ab initio parametrization of density functional dispersion correction (DFT-D) for the 94 elements H-Pu, *J. Chem. Phys.*, 2010, **132**, 154104.
5. C. Zuo, F. Chao, M. Li, Y. Dai, J. Wang, F. Xiong, Y. Jiang and Q. An, Improving Ca-Ion Storage Dynamic and Stability by Interlayer Engineering and Mn-Dissolution Limitation Based on Robust MnO_2@PANI Hybrid Cathode, *Adv. Energy Mater.*, 2023, **13**, 2301014.
6. Y. Chen, Z. Lu, T. Chen, Y. Liu, G. Han and G. Xu, Template-free hydrothermal synthesis of δ-MnO_2 hierarchical nanoflowers with potassium ions intercalation as cathodes for high-performing aqueous zinc ion batteries, *J. Electroanal. Chem.*, 2023, **929**, 117084.
7. D. Wang, Z. Liu, X.-W. Gao, Q. Gu, L. Zhao and W.-B. Luo, Massive anionic fluorine substitution two-dimensional δ-MnO_2 nanosheets for high-performance aqueous zinc-ion battery, *J. Energy Storage*, 2023, **72**, 108740.
8. H. Chen, W. Ma, J. Guo, J. Xiong, F. Hou, W. Si, Z. Sang and D. Yang, PEDOT-intercalated MnO_2 layers as a high-performance cathode material for aqueous Zn-ion batteries, *J. Alloys Compd.*, 2023, **93**, 167688.
9. N. Li, Z. Hou, S. Liang, Y. Cao, H. Liu, W. Hua, C. Wei, F. Kang and J.-G. Wang, Highly flexible MnO_2@polyaniline core-shell nanowire film toward substantially expedited zinc energy storage, *Chem. Eng. J.*, 2023, **452**, 139408.
10. M. Li, C. Liu, J. Meng, P. Hei, Y. Sai, W. Li, J. Wang, W. Cui, Y. Song and X.-X. Liu, Hydroxylated Manganese Oxide Cathode for Stable Aqueous Zinc-Ion

Batteries, *Adv. Funct. Mater.*, 2024, **34**, 2405609.

11. P. Chomkhuntod, K. Hantanasirisakul, S. Duangdangchote, N. Phattharasupakuna and M. Sawangphruk, The charge density of intercalants inside layered birnessite manganese oxide nanosheets determining Zn-ion storage capability towards rechargeable Zn-ion batteries, *J. Mater. Chem. A*, 2022, **10**, 5561–5568.
12. S. Zhou, X. Wu, H. Du, Z. He, X. Wu and X. Wu, Dual metal ions and water molecular pre-intercalated δ-MnO_2 spherical microflowers for aqueous zinc ion batteries, *J. Colloid Interface Sci.*, 2022, **623**, 456-466.
13. B. Cao, H. Liu, P. Zhang, N. Sun, B. Zheng, Y. Li, H. Du and B. Xu, Flexible MXene Framework as a Fast Electron/Potassium-Ion Dual-Function Conductor Boosting Stable Potassium Storage in Graphite Electrodes, *Adv. Funct. Mater.*, 2021, **31**, 2102126.